Author(s): Hirvasniemi, Jukka; Thevenot, Jérôme; Multanen, Juhani; Haapea, Marianne; Heinonen, Ari; Nieminen, Miika T.; Saarakkala, Simo

Title: Association between radiography-based subchondral bone structure and MRI-based cartilage composition in postmenopausal women with mild osteoarthritis

Year: 2017

Version:

Please cite the original version:

Hirvasniemi, J., Thevenot, J., Multanen, J., Haapea, M., Heinonen, A., Nieminen, M. T., & Saarakkala, S. (2017). Association between radiography-based subchondral bone structure and MRI-based cartilage composition in postmenopausal women with mild osteoarthritis. Osteoarthritis and Cartilage, 25(12), 2039-2046. https://doi.org/10.1016/j.joca.2017.09.008

Osteoarthritis and Cartilage 25 (2017) 2039–2046

Osteoarthritis and Cartilage

Association between radiography-based subchondral bone structure and MRI-based cartilage composition in postmenopausal women with mild osteoarthritis

J. Hirvasniemi † *, J. Thevenot ‡ §, J. Multanen ‖, M. Haapea ‡ ¶ #, A. Heinonen ††, M.T. Nieminen ‡ § ¶ #, S. Saarakkala ‡ § ¶ #

† *Center for Machine Vision and Signal Analysis, Faculty of Information Technology and Electrical Engineering, University of Oulu, Oulu, Finland*
‡ *Research Unit of Medical Imaging, Physics and Technology, Faculty of Medicine, University of Oulu, Oulu, Finland*
§ *Infotech Oulu, University of Oulu, Oulu, Finland*
‖ *Department of Physical Medicine and Rehabilitation, Central Finland Central Hospital, Jyväskylä, Finland*
¶ *Medical Research Center Oulu, Oulu University Hospital and University of Oulu, Oulu, Finland*
# *Department of Diagnostic Radiology, Oulu University Hospital, Oulu, Finland*
†† *Faculty of Sports and Health Sciences, University of Jyväskylä, Jyväskylä, Finland*

ARTICLE INFO

Article history:
Received 19 November 2016
Accepted 20 September 2017

Keywords:
Radiography
MRI
Osteoarthritis
Bone structure
Cartilage composition
Knee

SUMMARY

Objective: Our aim was to investigate the relation between radiograph-based subchondral bone structure and cartilage composition assessed with delayed gadolinium enhanced magnetic resonance imaging of cartilage (dGEMRIC) and T_2 relaxation time.

Design: Ninety-three postmenopausal women (Kellgren–Lawrence grade 0: $n = 13$, 1: $n = 26$, 2: $n = 54$) were included. Radiograph-based bone structure was assessed using entropy of the Laplacian-based image (E_{Lap}) and local binary patterns (E_{LBP}), homogeneity indices of the local angles ($HI_{Angles,mean}$, $HI_{Angles,Perp}$, $HI_{Angles,Paral}$), and horizontal (FD_{Hor}) and vertical fractal dimensions (FD_{Ver}). Mean dGEMRIC index and T_2 relaxation time of tibial cartilage were calculated to estimate cartilage composition.

Results: $HI_{Angles,mean}$ ($r_s = -0.22$) and $HI_{Angles,Paral}$ ($r_s = -0.24$) in medial subchondral bone were related ($P < 0.05$) to dGEMRIC index of the medial tibial cartilage. E_{Lap} ($r_s = -0.23$), $FD_{Hor,0.34\ mm}$ ($r = 0.21$) and $FD_{Ver,0.68\ mm}$ ($r = 0.24$) in medial subchondral bone were related ($P < 0.05$) to T_2 relaxation time values of the medial tibial cartilage. FD_{Hor} at different scales in lateral subchondral bone were related ($P < 0.01$) to dGEMRIC index ($r = 0.29$–0.41) and T_2 values of lateral tibial cartilage ($r = -0.28$ to -0.36). FD_{Ver} at larger scales were related ($P < 0.05$) to dGEMRIC index ($r = 0.24$–0.25) and T_2 values of lateral tibial cartilage ($r = -0.21$). $HI_{Angles,Paral}$ ($r = -0.25$) and $FD_{Ver,0.68\ mm}$ ($r_s = 0.22$) in the lateral tibial trabecular bone were related ($P < 0.05$) to dGEMRIC index of the lateral tibial cartilage.

Conclusion: Our results support the presumption that several tissues are affected in the early osteoarthritis (OA). Furthermore, they indicate that the detailed analysis of radiographs may serve as a complementary imaging tool for OA studies.

Introduction

Osteoarthritis (OA) is considered as a heterogeneous disease which affects all tissues in the joint and has several phenotypes[1–4]. In the articular cartilage, OA causes progressive degradation and loss of collagens and proteoglycans[5]. OA causes also changes in the density and structure of the subchondral bone[6–8].

* Address correspondence and reprint requests to: J. Hirvasniemi, Center for Machine Vision and Signal Analysis, Faculty of Information Technology and Electrical Engineering, University of Oulu, PO Box 4500, FI-90014 Oulu, Finland. Tel: 358-294-48-2778.

E-mail addresses: jukka.hirvasniemi@oulu.fi (J. Hirvasniemi), jerome.thevenot@oulu.fi (J. Thevenot), juhani.multanen@ksshp.fi (J. Multanen), marianne.haapea@oulu.fi (M. Haapea), ari.o.heinonen@jyu.fi (A. Heinonen), miika.nieminen@oulu.fi (M.T. Nieminen), simo.saarakkala@oulu.fi (S. Saarakkala).

https://doi.org/10.1016/j.joca.2017.09.008

In addition to semi-quantitative visual evaluation of the knee joint and measurement of cartilage thickness and volume, magnetic resonance imaging (MRI) can be used to assess the composition of the cartilage[9]. Compositional MRI techniques may be able to capture alterations in the biochemical properties of the tissue already in the early stage of the OA[9–11]. One of the currently available *in vivo* compositional MRI methods is T_2 relaxation time mapping. In the articular cartilage, the integrity and structure of the collagen network and water content affect T_2 relaxation time values[12,13]. Delayed gadolinium enhanced magnetic resonance imaging of cartilage (dGEMRIC) is another compositional MRI method and it has been widely used for the assessment of proteoglycan content of cartilage[11,13,14]. However, due to costs, availability of the MRI scanners and lengthy imaging time, MRI is not reasonable to be used as the first-line screening tool for OA or imaging of large cohorts.

Due to cheapness, fastness and good accessibility, plain radiography is suitable for imaging of large subject cohorts. Moreover, bone tissue is clearly visible on the radiographs. Fractal signature analysis (FSA) is a widely used method to assess bone structure from radiographs in OA research and it has been used to assess the progression of OA, for example[15–17]. We have previously shown that bone structure assessed from plain radiographs using Laplacian-based method, local binary patterns (LBP)-based methods, and FSA is significantly related with the actual 3-D microstructure of tibial bone[18]. We have also shown that subchondral and trabecular bone structures evaluated using LBP-based and Laplacian-based methods differ between subjects with different Kellgren–Lawrence (KL) grades[19]. However, the KL grading and structural analysis of bone were made for the same images in that study making the measurements dependent on each other to some extent, since features assessed in the KL grading, e.g., bone sclerosis, affect the bone structural parameters as well.

Consequently, to assess the sensitivity of the radiograph-based structural analysis of bone to early OA, the methods should be compared to compositional MRI. Therefore, the aim of this study is to investigate the linear relationships between radiograph-based subchondral bone structural parameters and cartilage composition, assessed with dGEMRIC and T_2 relaxation time, in postmenopausal women with or without mild OA.

Subjects and methods

Study subjects

Postmenopausal women ($n = 93$) without OA or with mild OA were included in this cross-sectional study (Table I)[20]. The inclusion and exclusion criteria were originally designed for exercise intervention study and have been published earlier (Table II)[20,21]. The knee with higher KL grade of the subjects with mild OA was selected for analysis (if both knees had the same KL grade, the most symptomatic knee was chosen), whereas the right knee of the subjects without OA was analyzed. The Ethics Committee of the Central Finland Health Care District approved the study design. Informed consent was obtained from all participants.

Acquisition of radiographs

Bilateral posterior–anterior weight-bearing knee radiographs were acquired with knees in a semi-flexed position (50 kVp, 1.25 mAs, pixel size: 170 × 170 μm^2, source-detector distance: 120 cm).

Table I
Description of the subjects ($n = 93$)

Parameter	Mean (standard deviation)	Min–max
Anthropometric variables		
Age (years)	58.3 (4.1)	50–66
Height (cm)	162.6 (5.9)	149–177
Weight (kg)	71.0 (10.8)	48–100
Body mass index (kg/m^2)	26.8 (3.7)	19–35
KL grade distribution		
KL0	13	
KL1	26	
KL2	54	

Selection of regions of interests (ROIs)

Four rectangle-shaped ROIs were extracted from the proximal tibia (Fig. 1). The locations of the ROIs were based on previous literature[18,19,22,23]. Two ROIs (size: 85 × 35 pixels, ~14 mm × 6 mm) were placed into the subchondral bone in the middle of the medial and lateral tibial plateaus immediately below the cartilage–bone interface. These ROIs are referred to as subchondral bone ROIs, although different bone types are mixed in the ROIs[6,8]. Furthermore, another two ROIs (85 × 85 pixels, ~14 mm × 14 mm), referred to as trabecular bone ROIs, were placed immediately below the dense subchondral bone area. Trabecular bone ROIs were aligned horizontally with subchondral bone ROIs. Some of the lateral trabecular bone ROIs were moved towards the center of the tibia to avoid overlapping with the fibula. Anatomical landmarks for the ROIs were tibial spine, subchondral bone plate, and outer borders of the proximal tibia. A custom-made MATLAB software (version R2014b, The MathWorks, Inc., Natick, MA, USA) was used for the manual placement (JH) of the ROIs. We have previously shown that the reproducibility of the texture parameters from the aforementioned locations is high[19]. Intra-observer reproducibility was high also in the current sample as the root-mean-square average coefficients of variations (CV_{RMS}) were below 1.7% for all texture parameters in all ROIs (data not shown).

Texture analysis of bone

Bone structure was evaluated from the radiographs using Laplacian-based method[18,19,24], LBP-based methods[18,25], and using FSA[18,22,26].

Table II
Inclusion and exclusion criteria for study subjects

Criteria
Inclusion
• Postmenopausal women.
• Age 50–65.
• KL grade 0, 1, or 2.
• Regular intensive exercise no more than twice a week.
• For subjects with KL1/KL2: knee pain on most days.
• For subjects with KL0: no any frequent pain, aching or stiffness in or around the knee joint in either knee in the preceding year.
Exclusion
• T-score for femoral neck bone mineral density lower than −2.5 g/cm^2 (i.e., indicating osteoporosis).
• Body mass index higher than 35 kg/m^2.
• Any previous knee instability or severe trauma.
• Illnesses that contraindicated exercise or limited participation in the exercise program.
• Inflammatory joint disease.
• Intra-articular steroid injections in the knee during the preceding 12 months.
• Contraindications to MRI.
• Allergies to contrast agents.
• Renal insufficiency.

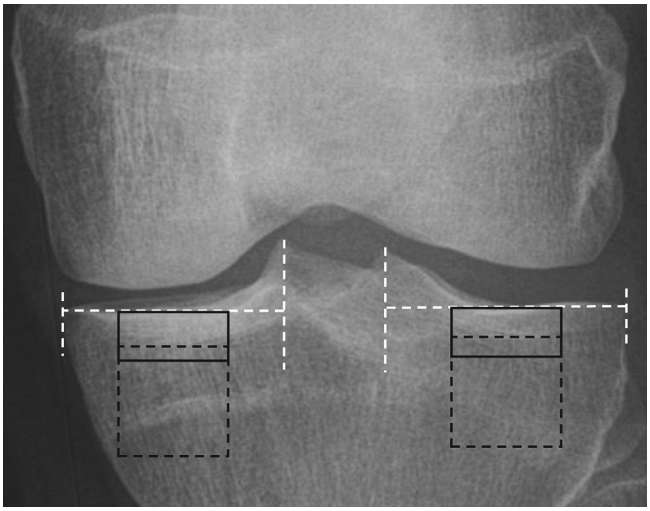

Fig. 1. Location of ROIs. Two ROIs (black rectangles with continuous line) were placed in subchondral bone immediately below the cartilage–bone interface in the middle part of the medial and lateral tibial plateaus and two ROIs (black squares with dashed line) immediately below the dense subchondral bone area. The purpose of the white dashed lines is to help place the ROIs in the middle of the tibial spine and outer border.

Laplacian-based analysis

The Laplacian-based method[18,19,24] enhances the appearance of bone trabeculae and quantifies the variation in the grayscale values of the Laplacian-based image. Laplacians were calculated in the horizontal and vertical directions and summed into the one matrix. The original ROI was multiplied with square root of the Laplacian matrix to enhance the visibility of the bone trabeculae and grayscale values were expanded to full dynamic range to obtain the final Laplacian-based image. To measure the randomness of the grayscale values in the Laplacian-based image, entropy of the image (E_{Lap}) was calculated using the following equation:

$$E = -\sum_i P_i \log_2 P_i, \quad (1)$$

where P_i contains the normalized count of the grayscale value i occurring in the image. If $E_{Lap} = 0$, all pixel values in the Laplacian-based image are the same, while higher values indicate higher variation in the pixel values of the image.

LBP-based methods

LBP-based methods were used to measure the randomness of local patterns and the variations in the orientation of adjacent local patterns. First, the image was divided into bone and non-bone regions by determining a local threshold for every image pixel using the Otsu method[27] with a 9 × 9 pixels window size. Next, the LBP operator (eight-neighborhood on a circle with a radius of 1) was applied in the bone regions and the bone edges (i.e., non-bone regions next to the bone). The pixel was considered to be an edge pixel if at least one of the eight neighbors of the center pixel was a bone pixel. Grouping of patterns was done by determining the main orientation and the number of valid neighbors (i.e., markers) for each pattern to reduce the number of irrelevant patterns. The main orientation angle (0°, 45°, 90°, and 135°) was calculated using principal component (PC) analysis only for the patterns consisting of 2–5 consecutive markers, otherwise the patterns were assigned as non-uniform.

To measure the randomness of the patterns occurring in the image, entropy of the grouped patterns (E_{LBP}) was determined using Equation (1). If $E_{LBP} = 0$, there is only a single pattern occurring in the image.

The homogeneity index (HI) for the orientation of the valid patterns was calculated from the co-occurrence matrix of the angles. The co-occurrence matrices were calculated in 0°, 45°, 90°, and 135° directions with one pixel distance. The non-uniform and non-bone areas were excluded from the co-occurrence matrices. To take into account the orientation of bone trabeculae in the analysis, co-occurrence matrices of 0° and 135° directions were combined together as well as 45° and 90° directions to calculate the HI perpendicularly to the bone trabeculae ($HI_{Angles,Perp}$) and along the trabeculae ($HI_{Angles,Paral}$), respectively. Furthermore, the mean HI ($HI_{Angles,mean}$) was calculated from the co-occurrence matrix as the sum of the four possible directions. The interpretation of the HI_{Angles} parameters used in this study is the following: if all adjacent patterns have similar orientation, HI_{Angles} is equal to one, while a large variation in the orientation of local patterns results in a low HI_{Angles} value.

FSA

FSA method was used to estimate fractal dimension[22,26]. In brief, the image was dilated and eroded in horizontal and vertical directions with a rod-shaped one-pixel wide structuring element. After that, the volume, V, between dilated and eroded images was calculated. Calculations were repeated by varying the element length r from 2 to 7 pixels. The surface area, $A(r)$, was obtained from Equation (2):

$$A(r) = (V(r) - V(r-1))/2. \quad (2)$$

Subsequently, a log–log plot was constructed by plotting log of $A(r)$ against log of r. Finally, the fractal dimension was estimated using a regression line to points in the plot and local fractal dimensions were obtained at 0.34 mm, 0.51 mm, 0.68 mm, and 0.85 mm sizes. When the structuring element is pointing in the horizontal direction, fractal dimension of vertical structures (FD_{Ver}) is produced and *vice versa*. High fractal dimension values are associated with high complexity of the image, whereas low complexity results in low fractal dimension values.

MRI

All subjects were scanned with a 1.5 T MRI scanner (Siemens Magnetom Symphony Quantum, Siemens Healthcare, Germany) with a standard transmit/receive knee array coil. T_2 relaxation time mapping was performed at the center of medial and lateral compartments using a fast-spin echo (FSE) sequence (repetition time (TR): 2090 ms, time to echo (TE): eight TEs between 13 and 104 ms, echo train length (ETL): 8, field of view (FOV): 140 × 140 mm^2, matrix: 256×256, slice thickness: 3 mm). One slice covering the central region of the condyle across sagittal view was chosen from the medial and lateral condyles for the analyses. Monoexponential fitting was used to compute T_2 relaxation time maps.

After T_2 measurements, dGEMRIC was performed at 90 min after intravenous administration of a double dose (0.2 mM/kg) of Gd-DTPA^{2-} (Magnevist, Schering, Berlin). Immediately after the injection of the contrast agent, subjects performed active flexion–extension exercises of the knee while sitting for 5 min, walking for 5 min and stair climbing for 5 min. Single-slice T_1 mapping was performed at the center of medial and lateral compartments using an inversion recovery FSE sequence (TR: 1800 ms, TE: 13 ms, inversion time: 50, 100, 200, 400, 800, and 1600 ms, ETL: 5, FOV: 140 × 140 mm^2, matrix: 256×256, slice thickness: 3 mm). The T_1 relaxation time maps were generated with a pixel-by-pixel three-parameter fit routine.

Articular cartilage was segmented manually for the quantitative T_1 and T_2 analyses using an in-house MATLAB application. The mean T_1, i.e., the dGEMRIC index, sensitive to cartilage proteoglycan content, and T_2 relaxation time, reflective of integrity of the collagen network and tissue hydration, were calculated for medial and lateral compartments from ROIs covering the whole tibial cartilage. In our laboratory, the intra-observer reproducibility (CV_{RMS}) of dGEMRIC is on average 7% for full-thickness ROIs and 5% for bulk cartilage[28] and the inter-observer reproducibility (CV_{RMS}) for T_2 and dGEMRIC full-thickness ROIs on average 2% and 3%, respectively[21].

Statistical analyses

The characteristics of the study population are shown as mean values with standard deviations. The normality of the parameters was assessed using Shapiro–Wilk test. The relationship between normally distributed parameters was evaluated using Pearson's correlation analysis (r) whereas Spearman's rank correlation (r_s) was applied if at least one of the parameters was not normally distributed. Absolute values of correlation coefficients were interpreted as follows: 0.00–0.19 very weak, 0.20–0.39 weak, 0.40–0.59 moderate, 0.60–0.79 strong and 0.80–1.00 very strong correlation[29]. No adjustments for multiple comparisons were performed[30].

Multiple linear regression analysis was performed to test how much the subchondral bone texture parameters together with clinical covariates (age, body mass index, and KL grade) explained the variation in the selected MRI parameter. Three different models were tested for selected MRI parameters in medial and lateral sides separately. Model 1 included clinical covariates and the bone texture parameter with the strongest correlation to the selected MRI parameter. As many texture parameters are correlated to each other, PC analysis was used for medial and lateral sides separately in the models 2 and 3. Model 2 included clinical covariates and PCs from FSA parameters (FD_{Hor} and FD_{Ver}) in subchondral bone. Model 3 included clinical covariates and all the calculated texture parameters in subchondral and trabecular bone ROIs. z-Transformed parameters ($z = (x - \mu)/SD$, where x is the value of each measurement, μ and SD are the average and standard deviation of the parameter to be transformed) were used. PCs explaining over 95% of the variance were selected for the regression analyses. As transitions between different KL grades might not be linear, we created a new binary variable describing KL grade by combining KL0 and KL1 to one group and used KL2 as another group. The number of predictors was limited to nine to avoid model overfitting. Only significant ($P < 0.05$) PCs (or at least one PC) were chosen for the final model. Residual analyses and multicollinearity diagnostics (variance inflation factors (VIF) were close to 1 for all models) were performed to assess quality of the each model. Statistical analyses were conducted using IBM SPSS Statistics for Windows (Version 22.0, IBM Corp., Armonk, NY, USA).

Results

In the medial compartment, $HI_{Angles,mean}$ ($r_s = -0.22$) and $HI_{Angles,Paral}$ ($r_s = -0.24$) (Fig. 2) in subchondral bone were weakly related ($P < 0.05$) to dGEMRIC index of the medial tibial cartilage

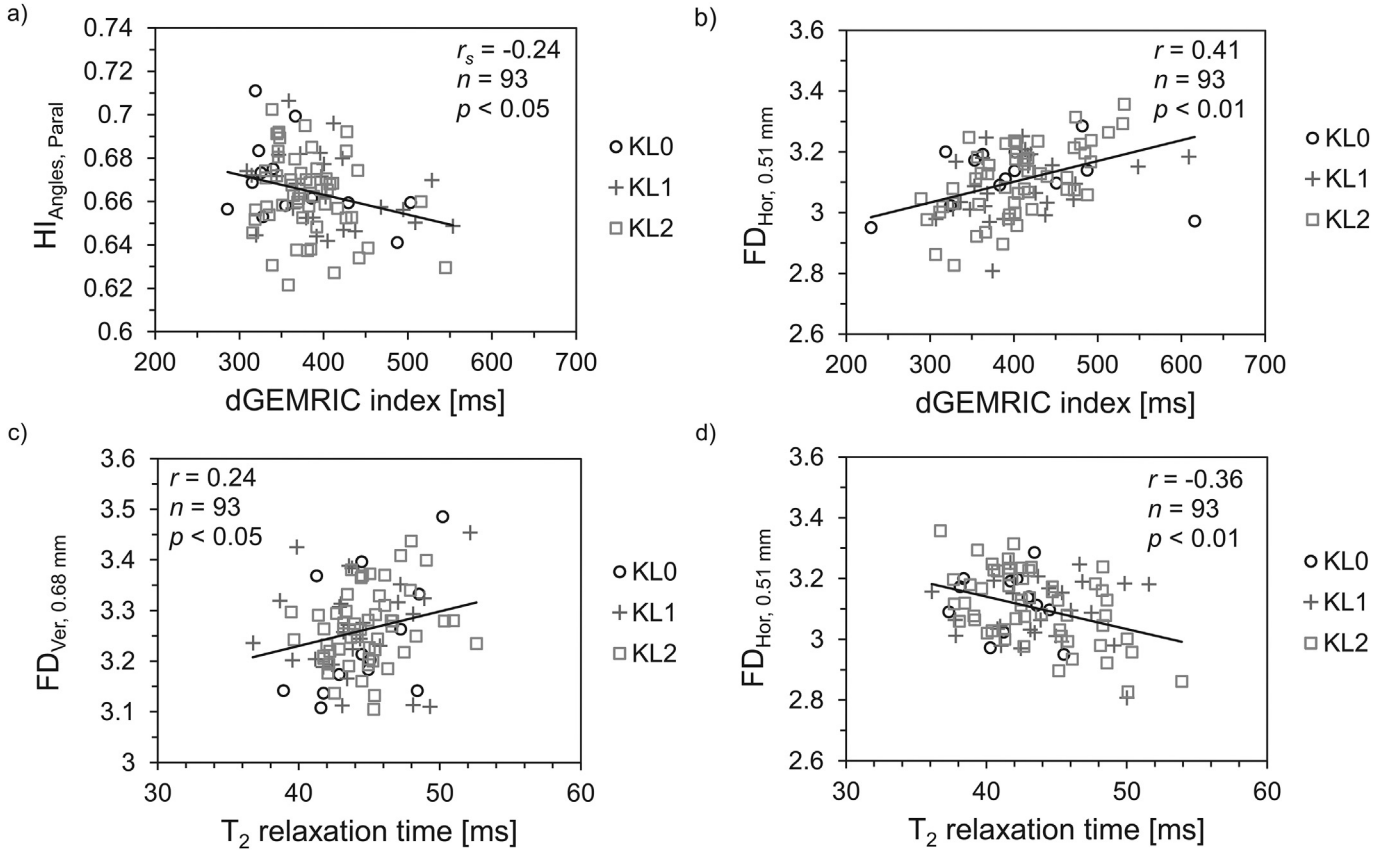

Fig. 2. Statistically significant correlations between (a) $HI_{Angles,Paral}$ in medial subchondral bone and dGEMRIC index of medial tibial cartilage, (b) $FD_{Hor,0.51\ mm}$ in lateral subchondral bone and dGEMRIC index of lateral tibial cartilage, (c) $FD_{Ver,0.68\ mm}$ in medial subchondral bone and T_2 relaxation time of medial tibial cartilage and (d) $FD_{Hor,0.51\ mm}$ in lateral subchondral bone and T_2 relaxation time of lateral tibial cartilage.

(Fig. 3). E_{Lap} ($r_s = -0.23$), $FD_{Hor,0.34\ mm}$ ($r = 0.21$) and $FD_{Ver,0.68\ mm}$ ($r = 0.24$) (Fig. 2) in medial subchondral bone were weakly related ($P < 0.05$) to T_2 relaxation time values of the medial tibial cartilage (Fig. 3). No associations were found between medial tibial cartilage composition and bone structural parameters in medial tibial trabecular bone (Fig. 3).

In the lateral compartment, FD_{Hor} in subchondral bone was weakly or moderately related ($P < 0.01$) to dGEMRIC index ($r = 0.29–0.41$) and T_2 values of lateral tibial cartilage ($r = -0.28$ to -0.36) (Figs. 2 and 3). FD_{Ver} at larger scales were weakly related ($P < 0.05$) to dGEMRIC index ($r = 0.24–0.25$) and T_2 values of lateral tibial cartilage ($r = -0.21$) (Fig. 3). Furthermore, $HI_{Angles,Paral}$ ($r = -0.25$) and $FD_{Ver,0.68\ mm}$ ($r_s = 0.22$) in the lateral tibial trabecular bone were weakly related ($P < 0.05$) to dGEMRIC index of the lateral tibial cartilage (Fig. 3).

The correlations between bone and cartilage parameters are summarized graphically for KL0/KL1 subjects ($n = 39$) in Supplementary Fig. 4 and for KL2 subjects ($n = 54$) in Supplementary Fig. 5. For KL0/KL1 subjects, $HI_{Angles,Paral}$ in medial subchondral bone was weakly related ($P < 0.05$) to dGEMRIC index of medial tibial cartilage ($r_s = -0.37$). For KL2 subjects, $FD_{Ver,0.51\ mm}$ ($r = 0.32$) in medial subchondral bone and E_{LBP} ($r = -0.27$) and FD_{Hor} ($r = 0.27–0.33$) in medial trabecular bone were weakly related ($P < 0.05$) to T_2 values of medial tibial cartilage. FD_{Hor} and FD_{Ver} at larger scales were weakly or moderately related ($P < 0.05$) to dGEMRIC index ($r = 0.33–0.59$) and T_2 values ($r = -0.30$ to -0.52) of lateral tibial cartilage.

T_2 relaxation time was not associated with dGEMRIC index in medial tibial cartilage ($r_s = -0.01$), whereas a weak association was detected in lateral tibial cartilage ($r = -0.27$, $P < 0.05$).

Regression models are summarized in Table III. Supplementary Table IV shows the loadings for PCs of FSA parameters in subchondral bone in medial and lateral sides. Supplementary Tables V and VI show the loadings for PCs of all texture parameters in subchondral and trabecular bone ROIs in medial and lateral sides, respectively. In medial side, model 1 ($HI_{Angles,Paral}$ in subchondral bone ROI, age, body mass index and KL grade) explained best the variation in dGEMRIC index ($R^2 = 0.146$, $P = 0.007$). Model 1 ($FD_{Ver,0.68\ mm}$ in subchondral bone ROI and the clinical covariates) explained best the variation in T_2 relaxation time ($R^2 = 0.071$, $P = 0.161$).

In lateral side, model 3 (four PCs of all texture parameters and the clinical covariates) explained best the variation in dGEMRIC ($R^2 = 0.278$, $P < 0.001$). Model 2 (two PCs of FSA parameters and the clinical covariates) explained best the variation in T_2 relaxation time ($R^2 = 0.158$, $P = 0.009$).

Discussion

In our current study, several statistically significant correlations between different radiograph-based bone structure-related parameters and cartilage composition assessed with dGEMRIC and T_2 relaxation time were found. The direction (positive/negative) of the correlations indicates that when tibial cartilage is degenerated, the underlying tibial bone structure is also deteriorated. However, the relation between subchondral bone structure and composition of cartilage was weak or moderate and not perfectly linear.

In medial tibial compartment, weak but significant correlation between subchondral bone structure ($HI_{Angles,mean}$ and $HI_{Angles,Paral}$) and dGEMRIC index of tibial cartilage was found. Additionally, E_{Lap}, $FD_{Hor,0.34\ mm}$ and $FD_{Ver,0.68\ mm}$ correlated weakly with T_2 relaxation time of medial tibial cartilage. In lateral subchondral bone, FD_{Hor}, and FD_{Ver} at larger scales, were weakly or moderately related to the dGEMRIC index and T_2 relaxation time values of the lateral tibial

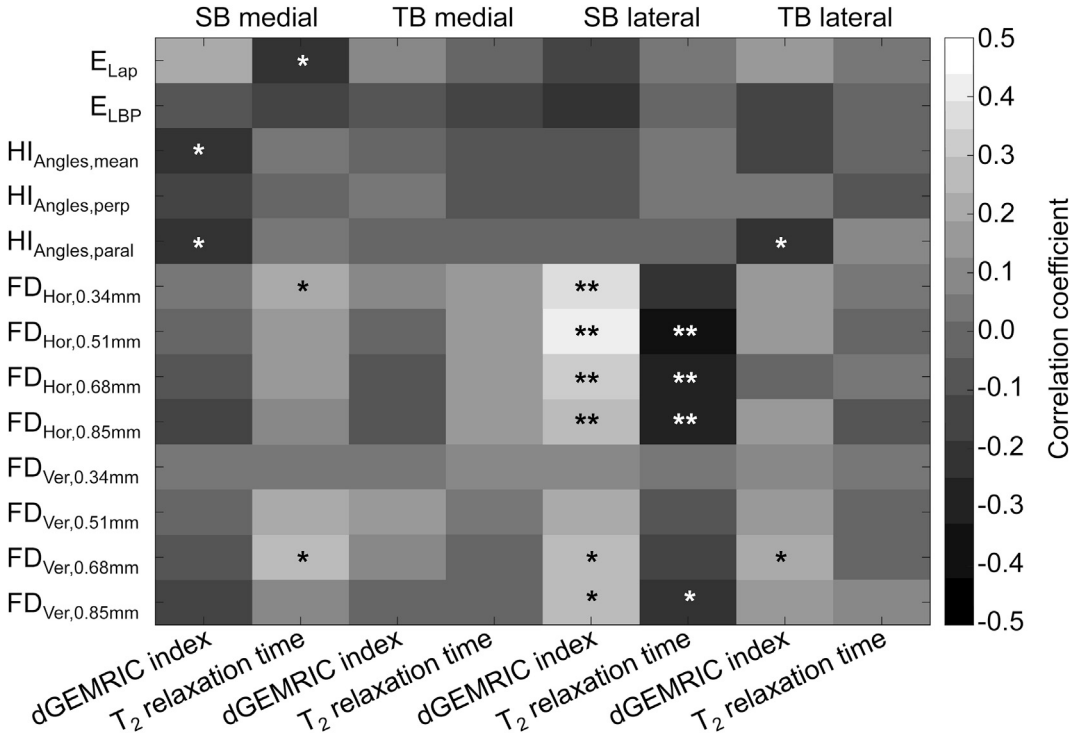

Fig. 3. Strength and direction of the correlation (Pearson's or Spearman's) between tibial cartilage composition and bone structure parameters in proximal tibia is color coded according to the grayscale bar. $n = 93$. $^*P < 0.05$, $^{**}P < 0.01$, SB = subchondral bone, TB = trabecular bone, E_{Lap} = entropy of Laplacian-based image, E_{LBP} = entropy of local binary patterns, $HI_{Angles,mean}$ = mean HI for orientation of local patterns, $HI_{Angles,Perp}$ = HI perpendicularly to the bone trabeculae, $HI_{Angles,Paral}$ = HI along the trabeculae, FD_{Hor} = fractal dimension of horizontal structures, FD_{Ver} = fractal dimension of vertical structures.

Table III
Regression models of the association between selected MRI parameter and selected ipsilateral bone structural parameters (model 1), selected PCs of the FSA parameters in subchondral bone (SB) (model 2) and selected PCs of all calculated bone structural parameters in subchondral and trabecular bone ROIs (model 3). All models were adjusted for age, body mass index and KL grade. $n = 93$

Dependent variable	Predictor	β	95% Confidence interval	P	Regression model	
					R^2	P
Medial compartment						
dGEMRIC index						
	Model 1:					
	$HI_{Angles,Paral}$ in SB	−0.301	−0.499 to −0.103	0.003	0.146	0.007
	Model 2:					
	$PC2_{FSA}$ in SB	−0.134	−0.339 to 0.071	0.197	0.075	0.141
	Model 3:					
	$PC3_{All}$	0.198	−0.004 to 0.400	0.055	0.092	0.062
T_2 relaxation time						
	Model 1:					
	$FD_{Ver,0.68\ mm}$ in SB	0.230	0.024 to 0.435	0.029	0.071	0.161
	Model 2:					
	$PC1_{FSA}$ in SB	0.211	0.001 to 0.422	0.050	0.061	0.229
	Model 3:					
	$PC2_{All}$	0.173	−0.040 to 0.387	0.111	0.047	0.368
Lateral compartment						
dGEMRIC index						
	Model 1:					
	$FD_{Hor,0.51\ mm}$ in SB	0.390	0.193 to 0.586	<0.001	0.196	0.001
	Model 2:					
	$PC1_{FSA}$ in SB	0.361	0.169 to 0.553	<0.001	0.225	<0.001
	$PC3_{FSA}$ in SB	0.208	0.017 to 0.399	0.033		
	Model 3:					
	$PC1_{All}$	0.255	0.065 to 0.444	0.009	0.278	<0.001
	$PC2_{All}$	0.263	0.080 to 0.446	0.005		
	$PC4_{All}$	0.194	0.009 to 0.379	0.040		
	$PC10_{All}$	−0.244	−0.428 to −0.060	0.010		
T_2 relaxation time						
	Model 1:					
	$FD_{Hor,0.51\ mm}$ in SB	−0.353	−0.557 to −0.150	0.001	0.135	0.012
	Model 2:					
	$PC1_{FSA}$ in SB	−0.245	−0.446 to −0.045	0.017	0.158	0.009
	$PC3_{FSA}$ in SB	−0.283	−0.482 to −0.084	0.006		
	Model 3:					
	$PC2_{All}$	−0.325	−0.523 to −0.126	0.002	0.123	0.020

cartilage. These results indicate that when the cartilage is degenerated, the structure of the underlying bone is also different. In general, when the cartilage is degenerated, more contrast agent is present in the cartilage and eventually the dGEMRIC index is lower[14]. Furthermore, elevated T_2 relaxation time values are associated with degenerated cartilage[11–13]. It should be noted that the radiograph-based bone structural parameters are dependent on the location of the ROI, since, e.g., the organization of the trabecular network is not similar in medially and laterally or in the subchondral bone and trabecular bone areas.

In the trabecular bone area, only $HI_{Angles,Paral}$ and $FD_{Ver,0.68\ mm}$ in the lateral side correlated significantly with the dGEMRIC index of the lateral tibial cartilage. This may indicate that the trabecular bone structure under the dense subchondral bone area (subchondral bone plate and subchondral trabecular bone) was not yet altered in this sample of postmenopausal women with mild OA, although cartilage was degenerated and changes in the subchondral bone were detected.

The multiple linear regression models explained the variation in the selected MRI parameter better in the lateral side. In addition regression models with one selected bone texture parameters, we used PC analysis to enable utilization of all fractal measures in subchondral bone area and all bone texture parameters from both ROIs in the regression analysis (many texture parameters are correlated to each other). In the lateral side, PCs related to fractal dimensions (in models 2 and 3) explained the most of the variation in both MRI parameters. For example, model 2 (constructed from PCs of FSA parameters in subchondral bone) had the highest coefficient of determination (R^2) to explain the variation in T_2 relaxation time. Furthermore, PC2 of all bone texture parameters was the most significant predictor of both MRI parameters in the lateral side. That component was strongly associated with FD_{Hor} in subchondral bone. These results are not surprising since, as the correlation analyses suggested, FD_{Hor} was associated with MRI parameters in the lateral tibia. It should be noted that the R^2-values of the regression models were low. Consistent with the current regression and correlation analyses, previous studies have reported more significant changes in the lateral side than in the medial side when comparing cartilage morphology[31–33], composition[32], or lesions[34] to the bone structure. Only one of the aforementioned studies assessed bone structure from radiographs[34]. In that study, fractal dimension of horizontal structures in the lateral compartment, and fractal dimension of vertical structures with small scales in both medial and lateral compartments, were significantly higher among subjects with cartilage defects (in medial, lateral, or both compartments) compared to subjects without defects detected with MRI[34]. Another one of the previously mentioned studies reported that MRI parameters related to cartilage composition ($T_{1\rho}$ and T_2) correlated negatively with MRI-based apparent bone volume fraction, trabecular thickness, and trabecular number and positively with apparent trabecular separation in the lateral side among subjects with mild OA and controls[32].

The relation between subchondral bone structure and composition of cartilage was not very strong and perfectly linear, which

was expected. One plausible reason for the relatively low correlations is that OA is a heterogeneous disease and likely has different origins. The selection of subjects with different OA phenotypes is challenging and it is probable that many phenotypes were mixed in our sample. Furthermore, it may be that not all tissues are affected in the early stage of the disease which may affect the correlation levels. Moreover, we investigated different tissues, i.e., cartilage using MRI and bone using radiographs, but the interplay between subchondral bone and articular cartilage is not clear yet. Estimation of the clinical significance of the results is challenging. Although statistically significant correlations between MRI-based cartilage composition and radiograph-based subchondral bone structure were observed, more detailed studies with carefully selected subjects (e.g., subjects that have or are at risk of developing bone changes) and imaging modalities are warranted in order to assess clinical relevance of the results and to further understand how and which factors affect the changes in the cartilage and subchondral bone.

This study contains certain limitations. Because of the cross-sectional study design, the causality of the tissue changes remains to be studied. For example, it was not possible to determine whether the changes in the cartilage composition induce the alteration in the subchondral bone structure or *vice versa*. One issue related to radiographs is that they are 2-D projection images of an object. However, 2-D radiograph-based bone density and structure have been shown to be significantly related with the actual 3-D structure of bone[18,35–38]. One limitation in the MRI-based methods is that they were done only for the single slice. It is possible for example that there were more degenerative changes outside the analyzed slice potentially reducing the level of correlation between cartilage and subchondral bone. Furthermore, although the dGEMRIC is regarded one of the best *in vivo* methods for the indirect measurement of the glycosaminoglycan content of the cartilage[11], the specificity of the method to glycosaminoglycan has been questioned[39–41]. However, the dGEMRIC method has been reported to detect degenerative changes of cartilage sensitively[14]. There are multiple comparisons in this study, and the results have to be viewed with certain provisos. However, we decided not to adjust for multiple testing[30].

In general, the results of the present study support the presumption that several tissues are affected in the early OA. The finding that cartilage composition and subchondral bone structure were related to each other shows that the detailed analysis of radiographs may serve as a complementary imaging tool for OA studies.

Authors' contribution

Conception and design: JH, MN, SS; acquisition of data: JH, JM, AH; analysis and interpretation of the data: all authors; drafting of the article: JH, SS; critical revision of the article for important intellectual content: all authors; final approval of the article: all authors.

Conflict of interest

The authors report no conflicts of interests.

Role of the funding source

The research leading to these results has received funding from Academy of Finland (projects 308165 and 268378), the Päivikki and Sakari Sohlberg Foundation, the Radiological Society of Finland, the Orion Corporation Research Foundation, the Sigrid Jusélius Foundation, and European Research Council under the European Union's Seventh Framework Programme (FP/2007–2013)/ERC Grant Agreement no. 336267. The funding sources had no role in the study design, data collection or analysis, interpretation of data, writing of the manuscript, or in the decision to submit the manuscript for publication.

Supplementary data

Supplementary data related to this article can be found at https://doi.org/10.1016/j.joca.2017.09.008.

References

1. Bijlsma JW, Berenbaum F, Lafeber FP. Osteoarthritis: an update with relevance for clinical practice. Lancet 2011;377:2115–26.
2. Glyn-Jones S, Palmer AJR, Agricola R, Price AJ, Vincent TL, Weinans H, *et al*. Osteoarthritis. Lancet 2015;386:376–87.
3. Karsdal MA, Christiansen C, Ladel C, Henriksen K, Kraus VB, Bay-Jensen AC. Osteoarthritis – a case for personalized health care? Osteoarthritis Cartilage 2014;22:7–16.
4. Pritzker KPH. Pathology of osteoarthritis. In: Brandt KD, Doherty M, Lohmander LS, Eds. Osteoarthritis. Oxford: Oxford University Press; 2003:49–58.
5. Buckwalter JA, Mankin HJ. Articular cartilage: degeneration and osteoarthritis, repair, regeneration, and transplantation. Instr Course Lect 1998;47:487–504.
6. Burr DB. Anatomy and physiology of the mineralized tissues: role in the pathogenesis of osteoarthrosis. Osteoarthritis Cartilage 2004;12:S20–30.
7. Goldring MB, Goldring SR. Articular cartilage and subchondral bone in the pathogenesis of osteoarthritis. Ann N Y Acad Sci 2010;1192:230–7.
8. Madry H, van Dijk CN, Mueller-Gerbl M. The basic science of the subchondral bone. Knee Surg Sports Traumatol Arthrosc 2010;18:419–33.
9. Roemer FW, Crema MD, Trattnig S, Guermazi A. Advances in imaging of osteoarthritis and cartilage. Radiology 2011;260:332–54.
10. Li X, Majumdar S. Quantitative MRI of articular cartilage and its clinical applications. J Magn Reson Imaging 2013;38:991–1008.
11. Oei EHG, Tiel J, Robinson WH, Gold GE. Quantitative radiologic imaging techniques for articular cartilage composition: toward early diagnosis and development of disease-modifying therapeutics for osteoarthritis. Arthritis Care Res (Hoboken) 2014;66:1129–41.
12. Mosher TJ, Dardzinski BJ. Cartilage MRI T_2 relaxation time mapping: overview and applications. Semin Musculoskelet Radiol 2004;8:355–68.
13. Nieminen MT, Nissi MJ, Mattila L, Kiviranta I. Evaluation of chondral repair using quantitative MRI. J Magn Reson Imaging 2012;36:1287–99.
14. Dahlberg LE, Lammentausta E, Tiderius CJ, Nieminen MT. *In vivo* monitoring of joint cartilage – lessons to be learned by delayed gadolinium enhanced magnetic resonance imaging of cartilage. Eur Musculoskelet Rev 2012;7:58–62.
15. Kraus VB, Feng S, Wang S, White S, Ainslie M, Brett A, *et al*. Trabecular morphometry by fractal signature analysis is a novel marker of osteoarthritis progression. Arthritis Rheum 2009;60:3711–22.
16. Kraus VB, Feng S, Wang S, White S, Ainslie M, Le Graverand M-H, *et al*. Subchondral bone trabecular integrity predicts and changes concurrently with radiographic and magnetic resonance imaging-determined knee osteoarthritis progression. Arthritis Rheum 2013;65:1812–21.
17. Janvier T, Jennane R, Valery A, Harrar K, Delplanque M, Lelong C, *et al*. Subchondral tibial bone texture analysis

predicts knee osteoarthritis progression: data from the Osteoarthritis Initiative. Osteoarthritis Cartilage 2017;25:259–66.
18. Hirvasniemi J, Thevenot J, Kokkonen HT, Finnilä MA, Venäläinen MS, Jämsä T, *et al*. Correlation of subchondral bone density and structure from plain radiographs with micro computed Tomography ex vivo. Ann Biomed Eng 2015;44:1698–709.
19. Hirvasniemi J, Thevenot J, Immonen V, Liikavainio T, Pulkkinen P, Jämsä T, *et al*. Quantification of differences in bone texture from plain radiographs in knees with and without osteoarthritis. Osteoarthritis Cartilage 2014;22:1724–31.
20. Multanen J, Heinonen A, Häkkinen A, Kautiainen H, Kujala UM, Lammentausta E, *et al*. Bone and cartilage characteristics in postmenopausal women with mild knee radiographic osteoarthritis and those without radiographic osteoarthritis. J Musculoskelet Neuronal Interact 2015;15:69–77.
21. Multanen J, Nieminen MT, Häkkinen A, Kujala UM, Jämsä T, Kautiainen H, *et al*. Effects of high-impact training on bone and articular cartilage: 12-month randomized controlled quantitative MRI study. J Bone Miner Res 2014;29:192–201.
22. Lynch JA, Hawkes DJ, Buckland-Wright JC. Analysis of texture in macroradiographs of osteoarthritic knees using the fractal signature. Phys Med Biol 1991;36:709–22.
23. Woloszynski T, Podsiadlo P, Stachowiak GW, Kurzynski M, Lohmander LS, Englund M. Prediction of progression of radiographic knee osteoarthritis using tibial trabecular bone texture. Arthritis Rheum 2012;64:688–95.
24. Thevenot J, Hirvasniemi J, Pulkkinen P, Määttä M, Korpelainen R, Saarakkala S, *et al*. Assessment of risk of femoral neck fracture with radiographic texture parameters: a retrospective study. Radiology 2014;272:184–91.
25. Thevenot J, Chen J, Finnilä M, Nieminen MT, Lehenkari P, Saarakkala S, *et al*. Local binary patterns to evaluate trabecular bone structure from micro-CT data: application to studies of human osteoarthritis. ECCV Workshops Part II. LNCS 2014;8926:63–79.
26. Lynch JA, Hawkes DJ, Buckland-Wright JC. A robust and accurate method for calculating the fractal signature of texture in macroradiographs of osteoarthritic knees. Med Inform (Lond) 1991;16:241–51.
27. Otsu N. Threshold selection method from gray-level histograms. IEEE Trans Syst Man Cybern 1979;SMC-9:62–6.
28. Multanen J, Rauvala E, Lammentausta E, Ojala R, Kiviranta I, Hakkinen A, *et al*. Reproducibility of imaging human knee cartilage by delayed gadolinium-enhanced MRI of cartilage (dGEMRIC) at 1.5 Tesla. Osteoarthritis Cartilage 2009;17:559–64.
29. Swinscow T. Statistics at Square One. 9th edn. London: BMJ Publishing Group; 1997.
30. Rothman KJ. No adjustments are needed for multiple comparisons. Epidemiology 1990;1:43–6.
31. Blumenkrantz G, Lindsey CT, Dunn TC, Jin H, Ries MD, Link TM, *et al*. A pilot, two-year longitudinal study of the interrelationship between trabecular bone and articular cartilage in the osteoarthritic knee. Osteoarthritis Cartilage 2004;12:997–1005.
32. Bolbos RI, Zuo J, Banerjee S, Link TM, Ma CB, Li X, *et al*. Relationship between trabecular bone structure and articular cartilage morphology and relaxation times in early OA of the knee joint using parallel MRI at 3T. Osteoarthritis Cartilage 2008;16:1150–9.
33. Lindsey CT, Narasimhan A, Adolfo JM, Jin H, Steinbach LS, Link T, *et al*. Magnetic resonance evaluation of the interrelationship between articular cartilage and trabecular bone of the osteoarthritic knee. Osteoarthritis Cartilage 2004;12:86–96.
34. Wolski M, Stachowiak GW, Dempsey AR, Mills PM, Cicuttini FM, Wang Y, *et al*. Trabecular bone texture detected by plain radiography and variance orientation transform method is different between knees with and without cartilage defects. J Orthop Res 2011;29:1161–7.
35. Le Corroller T, Pithioux M, Chaari F, Rosa B, Parratte S, Maurel B, *et al*. Bone texture analysis is correlated with three-dimensional microarchitecture and mechanical properties of trabecular bone in osteoporotic femurs. J Bone Miner Metab 2013;31:82–8.
36. Ollivier M, Le Corroller T, Blanc G, Parratte S, Champsaur P, Chabrand P, *et al*. Radiographic bone texture analysis is correlated with 3D microarchitecture in the femoral head, and improves the estimation of the femoral neck fracture risk when combined with bone mineral density. Eur J Radiol 2013;82:1494–8.
37. Ranjanomennahary P, Ghalila SS, Malouche D, Marchadier A, Rachidi M, Benhamou CL, *et al*. Comparison of radiograph-based texture analysis and bone mineral density with three-dimensional microarchitecture of trabecular bone. Med Phys 2011;38:420–8.
38. Steines D, Liew S, Arnaud C, Vargas-Voracek R, Nazarian A, Müller R, *et al*. Radiographic trabecular 2D and 3D parameters of proximal femoral bone cores correlate with each other and with yield stress. Osteoporos Int 2009;20:1929–38.
39. Salo EN, Nissi MJ, Kulmala KA, Tiitu V, Töyräs J, Nieminen MT. Diffusion of Gd-DTPA^{2-} into articular cartilage. Osteoarthritis Cartilage 2012;20:117–26.
40. Silvast TS, Kokkonen HT, Jurvelin JS, Quinn TM, Nieminen MT, Töyräs J. Diffusion and near-equilibrium distribution of MRI and CT contrast agents in articular cartilage. Phys Med Biol 2009;54:6823–36.
41. Stubendorff JJ, Lammentausta E, Struglics A, Lindberg L, Heinegard D, Dahlberg LE. Is cartilage sGAG content related to early changes in cartilage disease? Implications for interpretation of dGEMRIC. Osteoarthritis Cartilage 2012;20:396–404.